Chapter 3: Photophysics of covalently bridged naphthalene dimers

This chapter is devoted to the characterization of the excited states of covalent naphthalene dimers. In section 1, an introduction to previous works on related symmetric bichromophores are discussed, highlighting their interest for optoelectronic devices such as OPVs or OLEDs. The general objectives are outlined in section 2, followed by comments on the computational modeling in section 3. The results are discussed in section 4, to end with the general conclusions in section 5.

1. Introduction

Organic solar cells[1] are based on an heterojunction between a donor and an acceptor material, where the energy offset between the orbitals of these two materials is the driving force for charge separation. Upon light absorption, an exciton is created either in the donor or the acceptor layer. The mechanism of photocurrent generation due to exciton formation on the donor layer is illustrated in Figure 3.1. After the exciton is generated, it migrates to the donor/acceptor interface, where charge transfer takes place, generating a hole in the donor layer and an electron in the acceptor layer. Charge transport then takes place on each of the layers and the charges are eventually collected at the electrodes and transferred to the outer circuit.
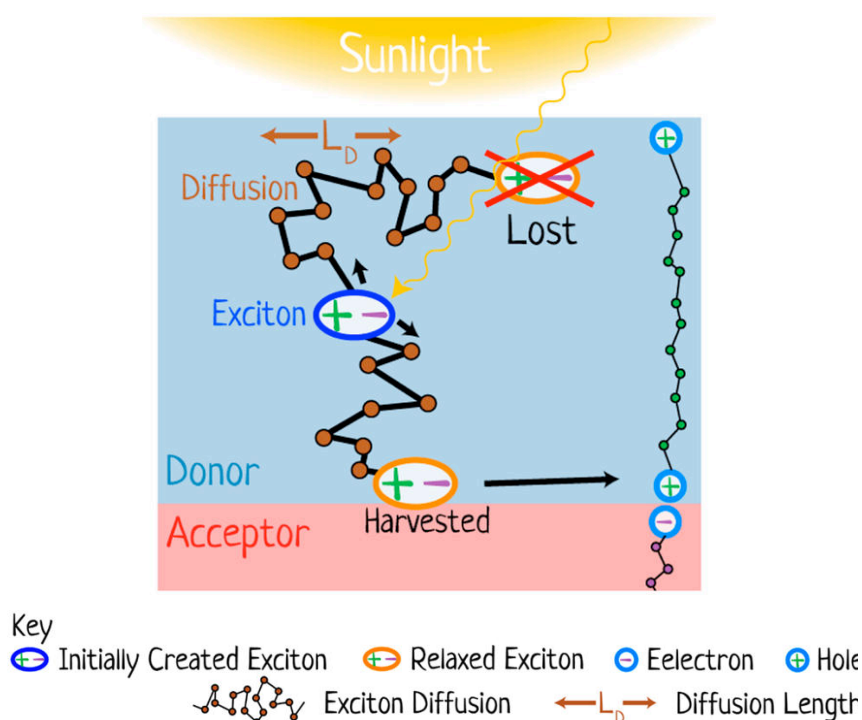
Figure 3.1 Schematic diagram of photocurrent generation in OPV devices. Incident sunlight leads to the formation of excitons that then diffuse to the heterojunction, where charge separation occurs. Some excitons do not reach the heterojunction and are lost. Taken from reference 1.

Organic photovoltaics represent a very promising alternative in the conversion of solar energy to electricity. Although they have the potential to provide electricity at a lower cost than solar technologies of the first and second generation, current record efficiencies (~13%)[2] are still far too low to compete with the performance of silicon panels[3] and other non-fossil energy sources. Organic solar cells present many advantages, i.e. abundance of materials, well-developed organic chemistry for their synthesis, available chemical strategies to tune their properties and the possibility of producing them as thin, flexible, and light weight modules that can be easily manufactured at room temperature. But in order for OPV technology to compete with other energy sources it is still necessary to overcome some fundamental obstacles. In particular, present OPV technologies exhibit short device lifetimes and low dielectric constants, resulting in low energy conversion efficiencies. One of the fundamental issues at the microscopic level is the generation of separated charges from the optical exciton, since high exciton binding energies result in important energy losses at the cell heterojunction that induce rather low open-circuit photovoltages (V_{oc}).

A promising and elegant strategy to increase V_{oc} values in OPVs is the use of symmetric molecular electron acceptors, such as covalent dimers of organic chromophores (bichromophores), able to undergo symmetry-breaking charge transfer (SBCT).[4-6] In SBCT, the initial excitation generated by photoabsorption relaxes to an intramolecular charge transfer state that breaks the molecular symmetry (Figure 3.2). Then, electron CT at the donor/acceptor interface leads to an oxidized donor and a reduced acceptor separated by a neutral chromophore, preventing fast charge recombination.

Organic bichromophores have also been proposed as highly emissive molecules for use in OLEDs[7,8] as an alternative to large aromatic molecules. In addition to strong photoluminescence, optimal molecular systems to be used in OLEDs must allow intermolecular CT.[9]
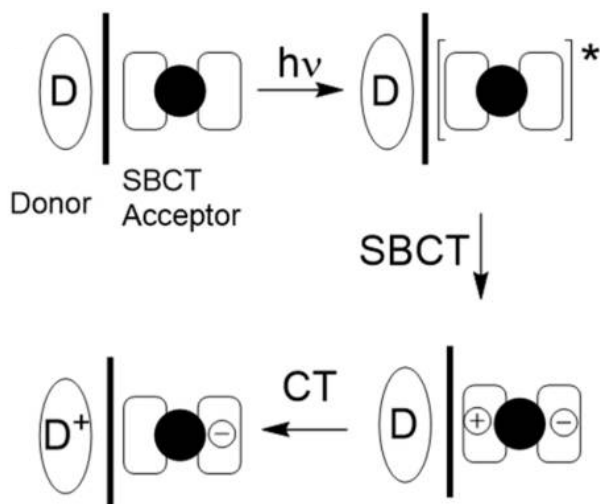
Figure 3.2 Schematic representation of the charge generation process in an OPV with a conventional donor (D) and a SBCT acceptor. First, an excited state is created through the absorption of a photon. Second, SBCT occurs on the molecule generating an intramolecular CT state. Finally, CT to the donor results in an oxidized donor (D^+) and a reduced acceptor ligand separated by a neutral acceptor ligand. If the excitation takes place in the bulk of the SBCT material, away from the D/A interface, the formed exciton must diffuse to the interface to charge separate. Taken from reference 6.

The range of applicability of bichromophores is expected to be related to the nature of the bridged monomers and their interaction. The electronic coupling between the conjugated moieties depends on the geometry and electronic structure of the covalent linker, and understanding the parameters that ultimately control and determine such interactions becomes critical to the design of molecular systems with the desired characteristics. Recently, it was shown that the covalent linkage between conjugated chromophores by a sulfur bridge has a large impact on the fluorescence efficiencies of the parent chromophores (Figure 3.3), with a large increase of PL yield with oxidation of the bridging sulfur atom, indicating a clear strategy in the search of new strong molecular emitters.[10] This trend was later scrutinized for the case of terthiophene dimers[11] in a study that concluded that rapid intersystem crossing to the triplet state manifold is the main deactivation process limiting the fluorescence quantum yield, as observed in pristine terthiophene.[12,13] The ISC efficiency is reduced in the presence of intramolecular CT, which can be tuned by the oxidation state of the bridging sulfur group. Electron lone-pairs on the sulfur atom screen the electronic interaction between the two chromophores, decreasing CT and allowing efficient ISC for the sulfide and sulfoxide dimers, and resulting in a larger PL efficiency for the sulfone bridge with no electron lone-pairs on the bridging S atom.
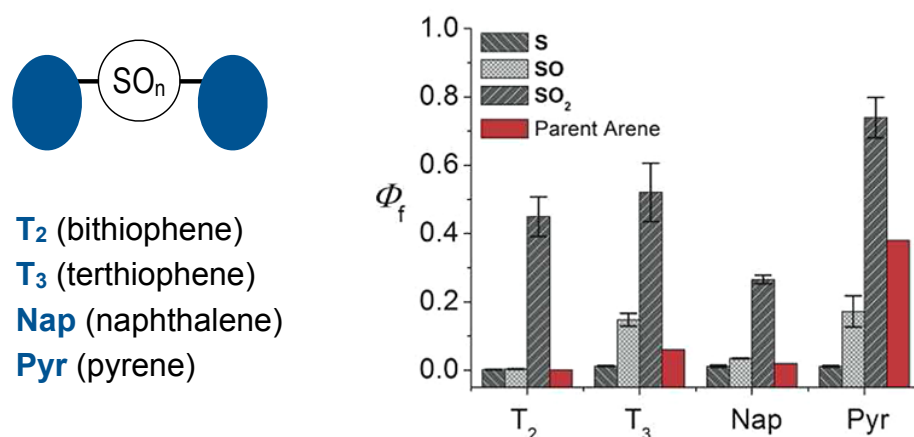
Figure 3.3 Left: sulfur bridged symmetric bichromophores based on sulfide (S), sulfoxide (SO) or sulfone (SO$_2$) with different organic chromophores (T$_2$, T$_3$, Nap, Pyr). Bar chart showing the increase in PL quantum yield (Φ_f) as the sulfur atom is oxidized in the covalent dimers. Values for the respective parent arenes are also shown. All measurements recorded in DCM solution. Taken from reference 10.

Despite the much less efficient ISC expected for naphthalene due to molecular planarity and the lack of sulfur atoms, PL in SO$_n$ bridged naphthalene dimers exhibits the same trend as in the terthiophene analogues. To understand the origin of such behavior and to further explore the validity of the lone-pair screening concept, we studied the photophysical properties of naphthalene covalent dimers (Figure 3.4) linked through the SO$_n$ bridge with n = 0, 1 and 2. These three molecules are labeled as **D0** (sulfide), **D1** (sulfoxide) and **D2** (sulfone) in the following.
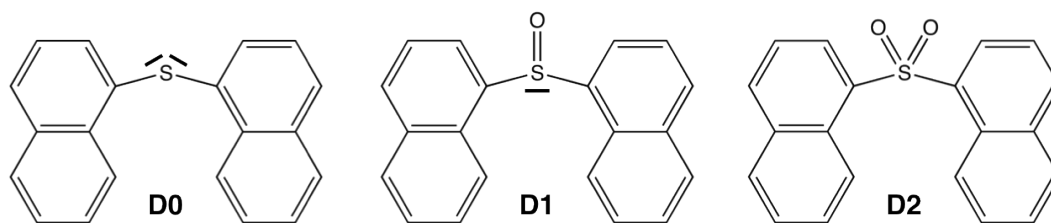
Figure 3.4 Molecular representation of the studied **Dn** dimers. Sulfur electron lone pairs are explicitly indicated.

2. General objectives

This work was mostly done during a research stay in the group of Prof. Mario Barbatti at the *"Institut de Chemie Radicalaire"* in Marseille (France). The main aim of this project was to give an explanation for the increase in PL quantum yield with increasing oxidation state of the sulfur atom from the bridge for the **Dn** dimers. We also wanted to check whether the lone electron pairs on the sulfur atom were able to screen interactions between the naphthalene moieties, as reported for analogous terthiophene dimers.[11]

First, the ground state of the **Dn** dimers was characterized by considering the relative stability of the structural conformers and their potential interconversion paths. Then the nature of the low-lying singlet states for the most stable conformers and the structural and electronic properties of local minima on the excited state energy surface were explored. Finally, the availability of non-radiative decay pathways from the lowest excited singlet to the ground state was considered.

3. Computational modeling

3.1 Default methods

Calculations of the **Dn** dimers were performed within the DFT and TDDFT frameworks. The (LRC) ωB97X-D functional[14] was chosen to properly describe excited states with CT contributions between the naphthalene moieties and the SO_n bridge, as well as to capture potential dispersion interactions between the two π-systems. The 6-31+G(d) basis set[15-17] was considered, since the use of diffuse functions might be qualitatively and quantitatively important in order to properly describe the electronic structure at the sulfur bridge and weak interactions between the naphthalene units. Preliminary calculations confirmed the importance of diffuse functions. Since the experimental data available for the **Dn** dimers was recorded in DCM solution, solvent effects were considered with the IEF-PCM[18,19] method.

3.2 Diabatic states

Due to the fact that the studied molecules are symmetric dimers, the analysis of the nature of the excited states by inspection of the MOs can be rather difficult, since in some cases they are delocalized over the entire molecule. Also, the low-lying excited states are described by several amplitudes where electrons are promoted from the HOMO and HOMO-1 to the LUMO and LUMO+1. These two sets of orbitals of the dimers are linear combinations of the HOMOs and LUMOs of each naphthalene fragment, respectively, with the occupied orbitals also having participation from lone pairs of the SOn bridge. Therefore, we use a diabatization procedure in order to characterize the low-lying transitions of the **Dn** dimers. Within this representation, the computed (adiabatic) excited states can be decomposed as linear combinations of contributions with a well defined physical nature, that is local excitations on each naphthalene, charge transfer excitations

between naphthalenes, and charge transfer excitations from the SOn bridge to the naphthalenes.

The two-fold adiabatic or diabatic representation of electronic states arises from the fact that the nuclear kinetic energy operator (T_{nuc}) and the electronic hamiltonian (H_{el}) do not commute. Therefore, these two operators do not have a common basis set. The eigenstates of H_{el} are the adiabatic states typically calculated with electronic structure codes, while the eigenstates of T_{nuc} are the diabatic states, which are less commonly used. Hence, adiabatic states are coupled by T_{nuc} via nonadiabatic couplings while diabatic states are electronically coupled (off-diagonal elements of H_{el}). It is important to point out that the nature of a diabatic state does not change with nuclear coordinates, since the off-diagonal terms of T_{nuc} in the diabatic representation are null, contrary to what happens for adiabatic states.

In 1982 Mead and Truhlar mathematically demonstrated[20] that, in general, diabatic states do not exist. This however does not impede an arbitrary definition of diabatic states for a given purpose. In the work presented herein, we chose the Edmiston-Ruedenberg diabatization scheme,[21] based on the maximization of the self-interaction of the diabatic states, in analogy to the MO localization technique.[22] Within this framework, diabatic states (Ξ) are obtained as linear combinations of adiabatic states (Φ) through a rotation matrix $\mathbf{U}$.

$$\left|\Xi_i\right\rangle = \sum_{j=1}^{N}\left|\Phi_j\right\rangle U_{ji} \qquad i = 1...N \qquad (3.1)$$

In practice, one has to select a finite number of adiabatic states that will represent the diabatic states of interest. Within this scheme, the electronic couplings between diabatic states can also be obtained as the off-diagonal terms of the diabatic electronic Hamiltonian.

3.3 S_0/S_1 crossings

3.3.1 Spin-flip DFT

In the work presented herein, S_0/S_1 energy crossings of the **Dn** dimers were investigated. Due to the failure of linear response TDDFT to describe these situations,[23] we decided to explore these regions of the PES using spin-flip DFT (SF-DFT) methods.[24] Within this methodology, spin α-to-β excitations are performed on a triplet reference state. In a two-

electrons-in-two-orbitals model, four spin eigenstates may be obtained by performing α-to-β excitations on the two unpaired electrons from a target $m_s=1$ triplet state: the ground and doubly excited closed shell singlets, the open shell singlet and the $m_s=0$ triplet. In the SF-DFT methodology, the presence of spin unbalanced excited determinants might cause spin-contamination for the computed ground and excited states.[25] Nevertheless, SF-DFT with hybrid functionals has proven to give good results for the characterization of conical intersections[26] involving the ground state.[27-29] Contrarily to TDDFT, in SF-DFT the ground state is coupled to the open shell singlet and both states are treated in a balanced way, since they are obtained as excitations from a triplet target state. We have used the BH&HLYP functional,[30,31] which contains 50% of HF exchange, since this is the recommended one to study conical intersections with SF-DFT methods.[27,29] It is important to point out that SF-DFT calculations with a pure xc functional are worthless since the excitation energies are simply orbital energy differences between α-occupied and β-virtual KS orbitals. In the SF-DFT methodology, HF exchange is necessary for single electron spin-flip excitations to be coupled.[24]

3.3.2 Crossing search and optimization

The S_0/S_1 energy crossings of the **Dn** dimers were found by chance when performing excited state optimizations with TDDFT. In the course of some optimizations, the energy gap between the first excited singlet state and the ground state became very small (< 0.10 eV). We then explored the S_0/S_1 energy gap for these geometries with SF-DFT and indeed the energy crossing was confirmed. We then performed (SF-DFT) geometry optimizations to locate the minimum energy crossing point (MECP) following the branching-plane updating algorithm[32] as implemented[33] in Q-Chem.[34] Within this methodology, the branching plane is approximated at each step by the normal difference vector and another vector that is orthogonal to it, avoiding the calculation of the derivative coupling vector. The energy along the seam is minimized by the gradient projection method,[35] where the optimization proceeds along a gradient vector that is projected onto the approximated seam space.

4. Results

4.1. Thermal conformers

The rotation around the S-naphthalene bonds of the studied molecules results in different conformations that might be energetically accessible depending on their relative stability and the experimental conditions. These structural conformers are local minima in the ground state PES of **Dn** dimers and correspond to different relative orientations between the naphthalene units and the oxygen atoms (Figure 3.5 and Appendix, Figure A3.1).

syn   *syn'*   *anti*   *perp*
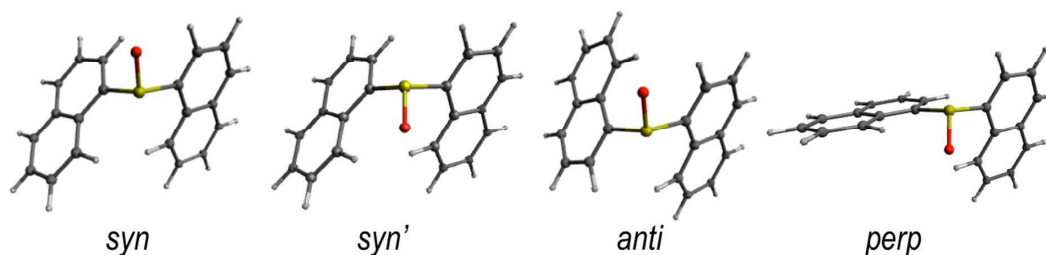
Figure 3.5 Lowest energy conformers for the ground state of the **D1** dimer. Low energy conformers of **D0** and **D2** are shown in the Appendix (Figure A3.1).

The energetically lowest forms of **D0** and **D1** in solution correspond to *syn* and *anti* arrangements of the naphthalene units with *syn* being slightly lower in energy (Table 3.1). As a result, it is reasonable to expect both conformers to be present in solution as computed by their Boltzmann fractions. On the other hand, **D2** shows a clear preference for the *anti* conformer, which is expected to largely be the main form in DCM solution.

It is worth noting that while **D0** only shows a sizeable net charge in any of its parts, i.e. the two naphthalene fragments or the sulfur bridge, in its *anti* conformer, the polarity of the S-O bond in the sulfoxide and sulfone bridges induces an electronic distribution towards the more electronegative O atoms (Table 3.1) for all conformers. Charge polarization in **D1** basically affects the SO linker, with S and O atoms carrying positive and negative charges, respectively. The presence of two O atoms in **D2** is able to pull considerable electron density from the two naphthalene units in the *syn* and *anti* conformers, resulting in a positive net charge on each chromophore. The different behavior of the *perp* form is related to the orthogonal orientation between naphthalene units, which results in asymmetrically charged chromophores.

Table 3.1 Relative energies ΔE (in kcal/mol), relative Boltzmann populations at T = 298K (Pop. in %) and Mulliken charges (q) on the S and O atoms, and on the naphthalene moieties for the ground state optimized structures of the lowest energy conformers (*conf.*) of **D0**, **D1** and **D2** dimers.

dimer	conf.	ΔE	Pop.	q(S)	q(O$_n$)	q(Napth$_2$)
D0	*syn*	0.0	74	0.00	-	0.00
	anti	0.7	23	0.20	-	-0.20
	anti'	1.8	3	-0.04	-	0.04
D1	*syn*	0.0	69	0.68	-0.69	0.01
	syn'	3.5	<1	0.48	-0.69	0.21
	anti	0.5	30	0.68	-0.71	0.03
	perp	2.8	<1	0.54	-0.69	0.14
D2	*syn*	2.5	1	0.18	-0.97	0.79
	anti	0.0	94	0.27	-0.95	0.68
	perp	1.8	5	0.92	-0.99	0.08

In addition to identifying and characterizing the low energy conformations of the naphthalene dimers, it is also important to quantify the barriers for their interconversion. The structural transformation between the low energy conformers of each dimer can be achieved by the torsion of one naphthalene moiety with respect to the other one. The ground state energy profiles for such mechanisms are shown in the Appendix (Figures A3.2-A3.4). The computed barriers for the molecular torsion between the low-lying conformers are in the 2-6 kcal/mol range.

In addition to the molecular torsion, the conversion between conformers of **D1** can be achieved by pyramidal inversion at the S atom (Figure 3.6). The transition states (TS) for the inversion of the *syn* and *anti* conformers exhibit a planar geometry around the sulfur atom with a naph-S-naph angle close to 120°, i.e. corresponding to a trigonal planar geometry, and much larger than the ground state angle (close to the tetrahedral angle). The computed inversion barriers for the *syn*→*syn'* and *anti*→*anti* conformational pathways are 38.4 and 38.6 kcal/mol, respectively, in quantitative agreement with computational estimations of the pyramidalization barrier computed for H_2SO, DMSO[36] and related sulfoxide heterodimers.[37] Hence, thermal pyramidal inversion of the sulfoxide dimer is expected to be very slow, as it has been previously observed for the racemization of aryl sulfoxides.[38,39] Analogously to the pyramidal inversion in **D1**, the *syn* and *anti* conformers of the **D2** dimer might convert into themselves by a tetrahedral inversion through the planarization of the sulfone center with a square planar transition state. Our calculations indicate that such geometry lies very high in energy (97 kcal/mol with respect to the

ground state *anti* conformer) and hence thermal interconversion of the sulfone-bridged naphthalene dimer via planarization can be completely disregarded. In spite of the lack of oxygen atoms in the **D0** bridge, it can also experience a similar inversion of the molecular structure by increasing the naph-S-naph angle at the bridge from the tetrahedral-like value (105°) in the *syn* and *anti* ground state minima to a linear C-S-C disposition. Again, the computational estimation of the energy barrier for the structural inversion of **D0** is too high (70 kcal/mol) to be thermally available, in very good agreement to the linearization energy estimated for H_2S.[40]
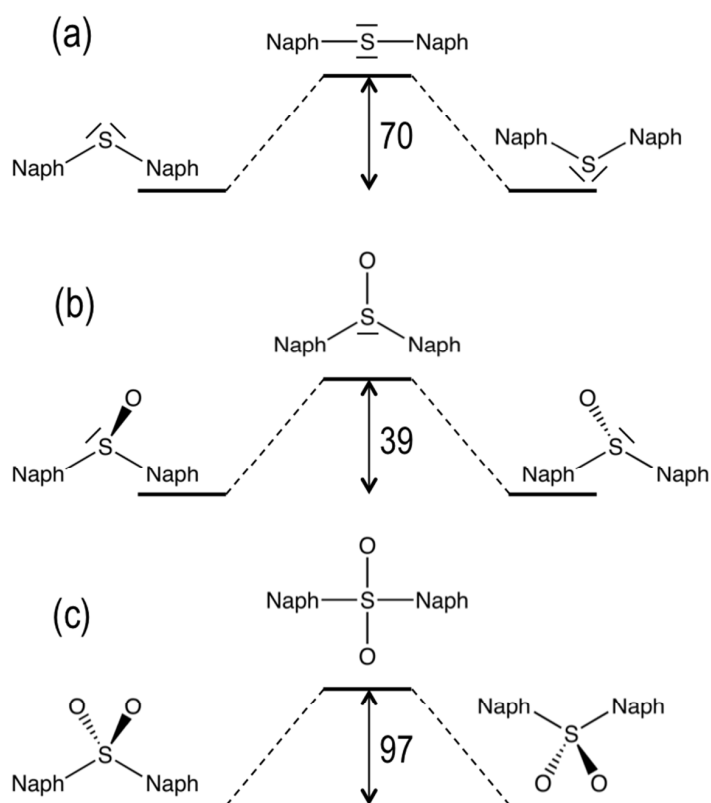
Figure 3.6 Ground state transition energy barriers (in kcal/mol) for the structural inversion of **D0** (a), **D1** (b) and **D2** (c) dimers. Molecular representations are only meant to indicate the main differences between S_0 and TS geometries. The nature of the S-O bond (single or double bond) has been omitted for the sake of clarity.

4.2. Photoabsorption

Computed vertical excitation energies from the ground state to the lowest excited singlet state of the **Dn** dimers are rather close to each other regardless of the oxidation state of the sulfur atom at the bridge and lie within the 4.2-4.4 eV range, in fairly good agreement with experimental absorption maxima measured in DCM solution (Table 3.2). Moreover, transition energies and oscillator strengths show small variations between different conformers.

Table 3.2 Vertical transition energies ΔE (in eV), oscillator strength (f), electronic character (in %) LE (on naphthalene fragments), CT (between naphthalene moieties) and CT_B (from the SO_n bridge to the naphthalenes), and electronic couplings between the lowest LE, CT and CT_B diabatic states (in meV) for the lowest excited singlet of the most stable conformers of the **D0**, **D1,** and **D2** dimers. Results for all computed conformers may be found in the Appendix (Table A3.1).

dimer	conf.	ΔE^a	f	LE	CT	CT_B	LE/CT	LE/CT_B
D0	syn	4.24	0.335	37	14	49	102	509
	anti	4.31	0.326	59	5	36	65	244
D1	syn	4.41	0.301	84	1	15	129	200
	anti	4.43	0.312	91	1	8	126	195
D2	anti	4.42	0.272	96	4	0	162	-

[a]Experimental absorption maxima : 4.11 eV (**D0**), 4.19 eV (**D1**) and 4.16 eV (**D2**). Values from reference 10.

The main contributions to the lowest electronic transition from the most stable conformations (*syn* and *anti*) of naphthalene dimers correspond to the single electron promotions from the two highest occupied molecular orbitals (HOMO and HOMO-1) to the two lowest unoccupied molecular orbitals (LUMO and LUMO+1). The frontier orbitals are mostly delocalized over the two naphthalene moieties with some contribution of the SO_n bridge, mainly for the HOMOs of the **D0** and **D1** molecules (Figure 3.7).
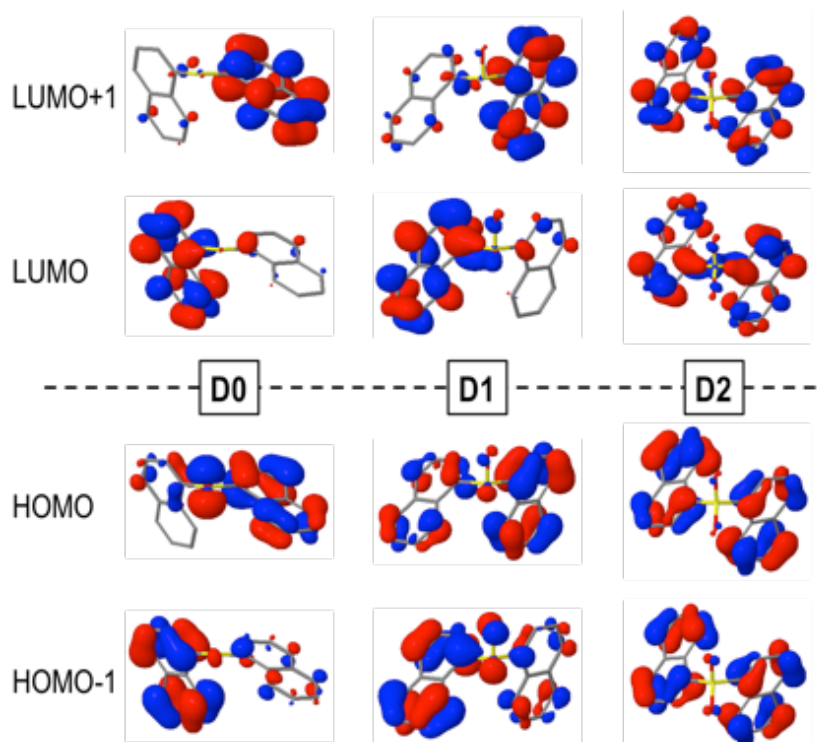
Figure 3.7 HOMOs (bottom) and LUMOs (top) of the *syn*-**D0** (left), *syn*-**D1** (middle) and *anti*-**D2** (right) dimers.

Despite the similarities between excitation energies and oscillator strengths for the $S_0 \rightarrow S_1$ transition in the **D0**, **D1** and **D2** dimers, a detailed electronic structure analysis brings to light soome significant differences in the nature of the transition upon oxidation of the bridge (Table 3.2). Decomposition of the electronic transition in terms of diabatic states corresponding to local excitations (LE) on the naphthalene moieties, charge transfer excitations between the aryl fragments (CT), and electronic transitions from the bridge to the naphthalene chromophores (CT_B) highlights important differences in the nature of the vertical excitation upon oxidation of the sulfur atom linker (Table 3.2). In general, the main contribution corresponds to $\pi \rightarrow \pi^*$ excitations on both naphthalene moieties, especially for the sulfone case. This contribution accounts for ~90% of the transition in **D1** and has proportionally a much lower role in the excitation of the **D0** conformers. This decrease of naphthalene-centered excitations is related to the larger involvement of the SO_n orbitals in the transition, corresponding to the electron lone pairs on the sulfur (**D0** and **D1**) and on the oxygen (**D1**) atoms, i.e. n(S) and n(SO) respectively. The presence of electron lone-pairs in the sulfide and sulfoxide linkers allows for sizeable CT_B contributions, related to the different electron density distributions found in the HOMOs (Figure 3.7). CT_B contributions are already rather important in **D1** (15% in the lowest *syn* conformer) and become the main contribution in *syn*-**D0** (49%). On the other hand, the lack of available lone-pairs forbids the bridge-to-naphthalene electronic transitions in the S_1 state of **D2**. For most of the cases, charge transfer between the two naphthalene fragments (CT) plays a minor role in the lowest excitation of **Dn** dimers. It is worth noticing that the LE/CT electronic coupling increases with the number of oxygen atoms in the bridge. This trend can be attributed to the electronic screening by the sulfur electron lone-pairs that limits the interaction between the two sets of π-electrons, as recently discussed for sulfur-bridged terthiophene dimers.[11] On the other hand LE/CT_B couplings are much larger for the sulfide than for the sulfoxide bridge in accordance with the amount of CT_B in the excitation, which can be rationalized as a result of the presence of one additional electron lone-pair in the former.

4.3. Fluorescent emission

Thorough computational searches of local minima on the lowest excited state PES of naphthalene dimers allowed us to identify a variety of states susceptible to decay back to the ground state via fluorescence emission (Table 3.3). The **Dn** dimers exhibit different structurally relaxed states corresponding to the stabilization of $\pi \rightarrow \pi^*$ excitations either

localized on one naphthalene unit (L) or delocalized over both conjugated chromophores (D), or to the optimization of CT excitations from the SO_n bridge (for n = 0 and 1) to the π* naphthalene empty orbitals (CT_B). The lack of sulfur lone-pairs prohibits the stabilization of CT_B states on the S_1 PES of **D2**, in line with the decomposition of the lowest excitation at the FC geometry (Table 3.2).

Table 3.3 Vertical deexcitation energy ΔE (in eV), oscillator strength *f*, Stokes shift (in eV) , and electronic character for the most stable conformers of the **D0**, **D1** and **D2** dimers. Relative stabilities between optimized excited states ΔE(rel) are also given (in kcal/mol). Labels in parenthesis for transitions involving π-type orbitals indicate localization on one naphthalene unit (L), delocalization over both naphthalene moieties (D) and excimer state nature (E).

dimer	*conf.*	character	ΔE(em)[a]	*f*	ΔE(Stokes)[b]	ΔE(rel)
D0	*syn*	π→π* (E)	3.12	0.110	1.12	6.7
	syn	*n*(S),π→π* (L)	3.58	0.316	0.66	1.9
	anti	*n*(S),π→π* (L)	3.39	0.215	0.85	2.6
	syn	*n*(S),π→π* (D)	3.51	0.325	0.73	2.1
	anti	*n*(S),π→π* (D)	3.43	0.322	0.81	0.0
D1	*syn*	π→π* (E)	2.95	0.078	1.45	0.0
	syn'	π→π* (E)	2.88	0.070	1.52	1.1
	anti	*n*(SO),π→π* (L)	3.65	0.191	0.76	3.7
	perp	*n*(SO),π→π* (L)	3.42	0.238	0.99	4.3
	perp'	*n*(SO),π→π* (L)	3.23	0.167	1.18	3.6
	syn	*n*(SO)→π* (D)	3.06	0.004	1.35	2.9
	anti	*n*(SO)→π* (D)	3.02	0.019	1.39	2.8
D2	*syn*	π→π* (E)	2.92	0.077	1.50	0.0
	anti	π→π* (L)	3.69	0.217	0.74	3.7
	perp	π→π* (L)	3.78	0.262	0.65	6.4

[a]Experimental emission maxima were obtained at 3.37 eV for the three dimers, while the measured Stokes shift was 0.74, 0.82 and 0.79 eV for **D0**, **D1** and **D2**, respectively.[10]
[b]Computed Stokes shift with respect to the vertical absorption of the most stable ground state conformer.

The *syn*-**Dn** dimers hold excited state minima with excimeric nature and molecular geometries with the two naphthalene units close to the coplanar eclipsed relative orientation (Appendix, Figure A3.5). These states present the largest Stokes shift for each dimer and are built from naphthalene π→π* excitations delocalized over the two chromophores without any involvement of the sulfur bridge. In addition, the large weights of CT excitations (50% of the transition) for these states unequivocally identify them as naphthalene excimers (Appendix, Figure A3.6). It is worth noting that while in **D0** the excimer is the energetically highest optimized excited state conformer, it is the most stable

state in **D1** and **D2**, with larger interstate gaps in the latter. Moreover, the adiabatic energy gap with respect to the ground state *syn* conformer decreases as **D0** > **D1** > **D2**, indicating stronger excimer stabilization for higher oxidation states of the bridge. The LE/CT couplings for the three *syn* excimers are computed at 626 (**D0**), 643 (**D1**) and 707 (**D2**) meV, considerably larger than the values for the FC structures and with a trend in accordance to the electron lone-pairs screening of the electronic interaction.

Excited states with the highest oscillator strengths for the naphthalene dimers correspond to $\pi \rightarrow \pi^*$ excitations localized on one naphthalene or to the mixing between $\pi \rightarrow \pi^*$ and $n(SO_n) \rightarrow \pi^*$ (**D0** and **D1**) excitations. Computed vertical emission energies and Stokes shifts for these states are in very good agreement with experimental measurements. The **D1** dimer also exhibits *syn* and *anti* low-lying states with virtually pure CT_B character and small oscillator strengths. Emission energies for $n(SO_n),\pi \rightarrow \pi^*$ (L) states are in very good agreement with PL frequencies and intensities computed for model systems with only one naphthalene unit (Appendix, Table A3.2), confirming the localized nature of the transition.

The excited state PESs along the molecular torsion between the two naphthalene moieties of the **Dn** dimers exhibit similar energy profiles to the ground state PES, with energy barriers for the conversion between different conformers within the 2-7 kcal/mol range (Appendix, Figures A3.2-A3.4). The energy profiles of the S_0 and S_1 PESs are rather parallel around the ground state local minima, suggesting that, depending on the experimental excitation conditions, two limiting situations might arise: (i) initial excitation does not modify the conformer population and the emitting states are entirely controlled by the ground state equilibria, or (b) the final emitting states are dictated by the relative stabilities between the minima in the S_1 PES (excited state equilibria). The latter situation would be closer to the case with excitation energies high enough to surpass torsion barriers. Simulated emission spectra in DCM for the two limiting situations are shown in Figure 3.8.

Estimation of relative photoluminescence (PL) quantum yields obtained from the integration of the emission profiles (Appendix, Table A3.3), either considering ground or excited state Boltzmann populations (Figure 3.8a and 3.8b respectively), indicate the **D0** dimer as the strongest emitter with a fluorescent efficiency being three to four times larger than in **D1** and **D2**. This result is in complete disagreement with experimental

observations, i.e. a much larger PL quantum yield (about one order of magnitude or more) in **D2** with respect to **D0** and **D1** dimers.[10] At this point, we must conclude that different state distributions over the computed S_1 minima cannot account for the different PL efficiencies between the sulfur-bridged naphthalene dimers, and that one or more non-radiative relaxation pathways (not considered so far) might play an important role in the deactivation of the excited **D0** and **D1** dimers. In the following, we explore potential non-radiative $S_1 \rightarrow S_0$ decay paths and rationalize why these mechanisms are favored in **D0** and **D1**, but not in **D2**, resulting in much larger emission intensity for the latter compound.
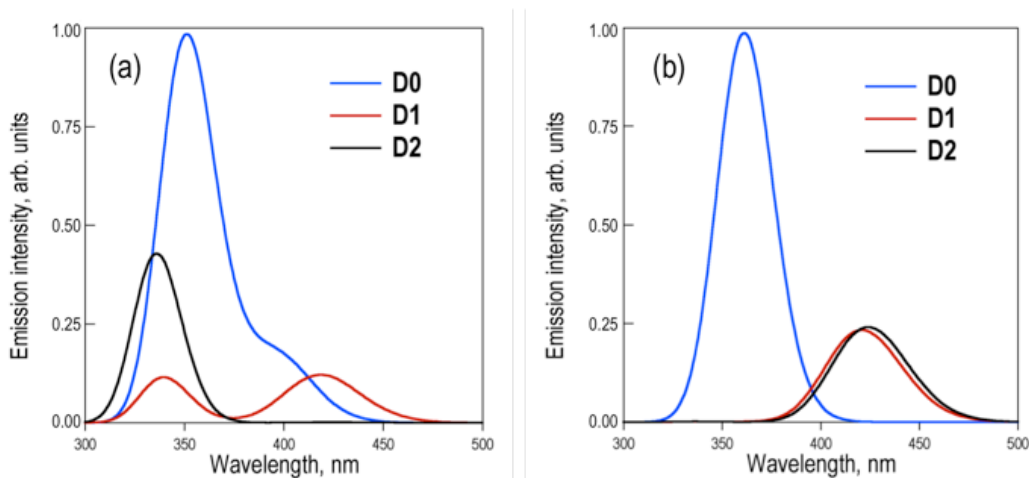
Figure 3.8 Simulation of emission spectra of **D0**, **D1** and **D2** dimers averaged over the ground state (a) and excited state (b) populations. Note that non-radiative decays have not been considered in the simulations.

4.4. Non-radiative relaxation pathways

First, we consider the possibility of an efficient internal conversion of the **D1** dimer following a pyramidal inversion mechanism on the excited state PES, as it has been proposed as a viable photo-induced process in aryl sulfoxides.[37] The energy barriers computed for the inversion of the *syn* and *anti* **D1** conformers are 3.5 and 3.0 kcal/mol, respectively, much lower than the energy required for the same structural rearrangement in the ground state (39 kcal/mol). Hence, it seems that the inversion might be thermally available after photoexcitation of the sulfoxide dimer. But in order for such a mechanism to result in an efficient IC to the ground state, strong non-adiabatic coupling between the two states is required. Since the interstate couplings are inversely proportional to the energy gap, a small energy difference between the two PESs is necessary. Estimation of the S_0/S_1 energy gaps at the inversion TS are computed as 32 and 50 kcal/mol for the *syn* and *anti* conformers, respectively (Appendix, Table A3.4). Hence, despite the availability of the

photo-induced pyramidal inversion in **D1**, the magnitude of the S_0/S_1 gaps forces us to discard an efficient non-radiative decay via IC at the inversion TS. Although the computed tetrahedral inversion barrier for **D2** in the lowest excited state is also considerably much lower than in the ground state, i.e. 41 vs. 97 kcal/mol, in this case the barrier is still too large to allow for photo-induced tetrahedral inversion. Furthermore, the S_0/S_1 energy gap at the TS is estimated at 29 kcal/mol, blocking the non-radiative decay to the ground state via IC. Similar results have been obtained for the energy difference between the two states of **D0** at the inversion TS, i.e. 14 kcal/mol and 11 kcal/mol for the *syn* and *anti* conformers, respectively.

In an attempt to find potential efficient non-radiative mechanisms for the photo-excited naphthalene dimers, we explored regions of the PES where the gap between the ground and lowest excited singlet states becomes small or where the two states become degenerate, that is S_0/S_1 intersections. For the sake of clarity, in the following we only discuss the results regarding the most stable conformations, that is *syn* (**D0** and **D1**) and *anti* (**D2**) forms. Indeed, for **D1** we identify a molecular geometry with a trigonal planar arrangement of the SO_1 bridge that is structurally related to the TS of the pyramidal inversion, where the ground and excited PESs intersect with non-vanishing non-adiabatic couplings at the proximity of the crossing (see Appendix), i.e. a conical intersection. At this intersection that we label as *sym*-CI, there is a symmetric elongation of the S-C bonds between SO_1 and the naphthalene units and an important increase of the bridge C-S-C angle (Table 3.4). More importantly, the *sym*-CI point lies ~0.66 eV below the S_1 state at the FC region, thus it is energetically accessible upon photoexcitation, providing a clear molecular mechanism to relax back to the ground state without photoemission. Similarly, we obtain a symmetric state crossing for the **D0** dimer, which exhibits a similar geometrical pattern (long C-S bonds and linear C-S-C angle). But, in this case, the *sym*-CI is obtained energetically above the FC S_1 energy. For both dimers, **D0** and **D1**, at the *sym*-CI the ground state crosses with the $n(SO_n) \rightarrow \sigma^*$ state, which is stabilized by the elongation of the two S-C bonds (Figure 3.9). Moreover, in **D1**, the planarization of the sulfoxide group destabilizes the $n(SO)$ orbital due to π *anti*-bonding interaction with the p_z orbital of the oxygen atom. In the **D0** dimer, the $n(S)$ destabilization comes from the interaction with the π-orbitals of coplanar naphthalene fragments. On the other hand, the lack of electron lone-pairs in the sulfone bridge inhibits the presence of a low energy *sym*-CI in the **D2** dimer.

Table 3.4 Structural parameters (in Å and degrees) and relative energies (in eV) with respect to the S_1 energy at the FC region of the inversion TS (*inv*-TS), and the *sym*-CI and the *asym*-CI points for the *syn* conformers of **D0** and **D1** dimers.[a]

dimer	state	r(C-S)	α(C-S-C)	ΔE(rel)
D0	*inv*-TS	1.80/1.80	178	+0.60
	sym-CI	2.17/2.12	178	+0.68
	asym-CI	2.26/1.77	176	-0.23
D1	*inv*-TS	1.76/1.76	115	+0.15
	sym-CI	1.96/1.88	155	-0.66
	asym-CI	2.32/1.78	107	-1.03

[a]Geometries for the *sym*-CI and *asym*-CI can be found in Appendix (Figure A3.7)

Excited state optimization within the CI subspace, i.e. minimal energy CI (MECI) searches, of sulfide and sulfoxide dimers result in non-symmetric molecular geometries (*asym*-CI) with one rather long S···C distance and a short S-C bond. As a result, the σ* MO localizes on one side of the dimer (at the long S···C separation). This structural arrangement suggests a path towards molecular fragmentation. Furthermore, the computed *asym*-CI energies lie below the S_1 energy at the FC region (and below the *sym*-CI point), and are therefore energetically available for both dimers. Hence, we identify the non-adiabatic relaxation of **D0** and **D1** dimers through *asym*-CI as the mechanism describing reversible molecular fragmentation (although the molecule has not been effectively fragmented in *asym*-CI), where there is an elongation and shrinking of a S-C bond resulting in a fast decay to the electronic ground state. The reverse fragmentation mechanism has been proposed as the main inversion of aryl sulfoxides with a 1° alkyl group.[36,38,39,41] Moreover, we find that such a mechanism can be potentially photoinduced in sulfide and sulfoxide aromatic dimers and that it proceeds through a MECI.
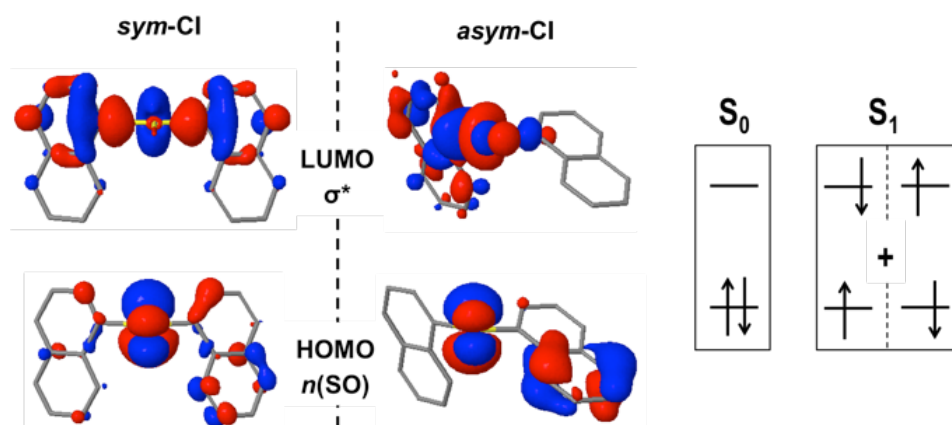
Figure 3.9 Frontier molecular orbitals n(SO) and σ* at the S_0/S_1 *sym*-CI and *asym*-CI points for the sulfoxide naphthalene dimer (**D1**).

By gathering the results discussed above regarding the photoexcitation and different deactivation paths of the studied naphthalene dimers, it is possible to draw a general picture for the photophysical properties of **Dn** dimers. The main photophysical mechanisms explored are represented in the Jablonski diagram of Figure 3.10. Relaxation of the photo-excited sulfur-bridged naphthalene dimers allows the formation of strongly emissive localized excitations and weakly emitting excimers. Moreover, sulfide and sulfoxide dimers exhibit non-radiative decays back to their ground states, which actually dominate their excited state dynamics in solution. On the other hand, the lack of electron lone-pairs in **D2** blocks the presence of excited to ground state crossings, resulting in much larger PL yields with respect to those in **D0** and **D1**.
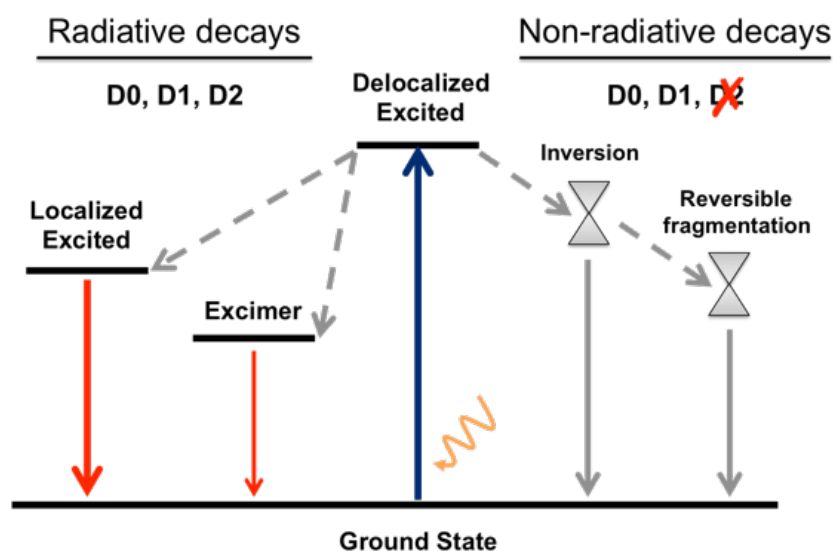
Figure 3.10 General Jablonski diagram for the deactivation mechanisms after photoexcitation of **D0**, **D1,** and **D2** naphthalene dimers.

5. Conclusions

In this work we have identified and characterized both radiative and non-radiative deactivation mechanisms in sulfur-bridged naphthalene dimers. The different PL efficiencies upon oxidation of the bridge have been rationalized by the existence of energetically available, non-radiative decay paths for the sulfide and sulfoxide bridges. The lack of electron lone-pairs in the sulfone linker is the origin of the much stronger PL with respect to S and SO cases.

Although the computed vertical transition energies and their intensities at the FC structures are very similar for the three naphthalene dimers, there are sensible differences in the character of the transition to the lowest excited singlet between **D0**, **D1,** and **D2**, that is a

larger involvement of the $n(SO_n)$ orbitals in terms of bridge→naphthalene CT with lower oxidation state of the sulfur atom. Geometrical relaxation to local minima of the excited state PESs cannot account for the very weak PL of **D0** and **D1**, pointing towards the existence of efficient non-radiative decays, not present for excited **D2** molecules. We identify energy crossing regions for the **D0** and **D1** dimers allowing the conversion of the photo-excited molecules back to the ground state with no fluorescence emission. Our calculations indicate that while two types of S_0/S_1 state crossings, i.e. symmetric and asymmetric, might be reached along the excited state decay of **D1**, only the asymmetric intersection is energetically available in the **D0** dimer. The identification of an energetically available asymmetric CI pointing towards the reversible molecular fragmentation, suggests a photo-induced roaming mechanism[42] as a potential non-radiative deactivation path for **D0** and **D1**. Finally, it is important to notice that in our calculations, due to the nature of the studied chromophores, we have not considered the role of ISC as one of the main deactivation channels.

The present results suggest that, differently to the terthiophene dimers, the SO_n bridged naphthalene bichromophores do not require efficient ISC to limit their fluorescence emission. On the other hand, our results reinforce the generality of the electron lone-pair screening concept for sulfur-bridged chromophore dimers. The obtained results and conclusion are general enough to be extrapolated to other sulfur-bridged conjugated dimers, therefore proportionating novel strategies in the design of strong photoluminescent organic molecules with controlled charge transfer.

6. Appendix

6.1 Computational details

Electronic structure calculations for ground and excited states were performed within the DFT[43,44] and the TDDFT[45,46] frameworks, respectively. To take into account weak interactions and the important electronic redistribution between the naphthalene moieties and the SO_n bridge upon photoexcitation, the ωB97X-D functional[14] was used together with the 6-31+G(d) basis set.[15-17] Investigations on the dependence of the energy functional and basis set can be found in the Appendix (Tables A3.5 and A3.6). DCM solvent effects were taken into account with the IEF-PCM method.[18,19] Critical points on the ground state PESs were optimized with no restrictions and characterized within the harmonic

approximation. The simulated emission spectra were calculated by convolution of Gaussian functions (half-bandwidth of 2500 cm^{-1}) centered at the computed vertical emission energies of all excited state minimum and were averaged according to ground or excited state Boltzmann populations (based on relative electronic energies). Computation of diabatic states was obtained by means of the Edmiston-Ruedenberg localization[21] scheme. Energy crossing points and derivative couplings between S_0 and S_1 were computed using the spin-flip DFT (SF-DFT) approximation[24] with the BH&HLYP functional.[30,31] All calculations were performed with the Gaussian09 package, revisions B01 and D01,[47] and the Q-Chem program.[34]

- **Transition states for the structural inversion**

The transition states for the structural inversion of **D1** and **D2** were characterized as first order saddle points, while those of **D0** were second order saddle points on the ground state PES. This second order saddle point which corresponds to a linear structure of **D0** is a transition state connecting two transition states (first order saddle points). These latter transition states connect the two enantiomers of *syn* and *anti* ground state conformers respectively.

- **CI relative energies**

The values of ΔE(rel) for *inv*-TS and *sym*-CI (Table 3.4 of the main text) were calculated within the TDDFT. The values of ΔE(rel) for *asym*-CI were calculated by the following expression, since TDDFT cannot properly describe the situation of bond fragmentation.

ΔE(rel) = Δ*sym* + Δ*asym*

Δ*sym* = ΔE(rel) for *sym*-CI

Δ*asym* = relative energy of *asym*-CI with respect to *sym*-CI calculated by SF-DFT

- **Derivative couplings**

Derivative couplings (atomic units) for the **D0** and **D1** dimers.

sym-CI	**D0**	71.3
	D1	169.8
asym-CI	**D0**	5550.8
	D1	2644.5

Note. The derivative coupling vectors correspond to the same nuclear motion as the imaginary frequencies of the transition states of **D1** and **D0**. Therefore, the nuclear motion that lowers the energy from the transition states to the ground state minima is equivalent to the motion that opens the gap of the S_1/S_0 crossing.

Table A3.1 Vertical transition energies ΔE (in eV), oscillator strengths (f), electronic character (in %) LE (on naphthalene fragments), CT (between naphthalene moieties) and CT_B (from the SO_n bridge to the naphthalenes), and electronic couplings between the lowest LE, CT and CT_B diabatic states (in meV) for the lowest excited singlet of the different conformers of the **D0**, **D1** and **D2** dimers.

dimer	*conf.*	ΔE^a	f	LE	CT	CT_B	LE/CT	LE/CT_B
D0	*syn*	4.24	0.335	37	14	49	102	509
	anti	4.31	0.326	59	5	36	65	244
	anti'	4.37	0.347	68	9	23	119	149
D1	*syn*	4.41	0.301	84	1	15	129	200
	syn'	4.35	0.280	78	4	18	98	221
	anti	4.43	0.312	91	1	8	126	195
	perp	4.33	0.329	44	11	45	128	153
D2	*syn*	4.38	0.273	94	6	-	121	-
	anti	4.42	0.272	96	4	-	162	-
	perp	4.47	0.341	100	0	-	41	-

[a]Experimental absorption maxima: 4.11 eV (**D0**), 4.19 eV (**D1**) and 4.16 eV (**D2**). Values from reference 10.

Table A3.2 Vertical transition energies ΔE (in eV) and oscillator strengths (f) for the naphthalene-SO_n-Me molecules.

SO_n	geometry	ΔE	f
S	S_0	4.53	0.18
	S_1	3.50	0.23
SO	S_0	4.52	0.19
	S_1	3.73	0.20
SO$_2$	S_0	4.52	0.18
	S_1	3.81	0.21

Table A3.3 Estimated relative PL quantum yields (without considering non-radiative decay pathways) obtained as the numerical integration of the emission profiles of the **Dn** dimers considering (i) a ground state population (S_0) and (ii) an excited state population (S_1) compared to the experimental yields taken from reference 10.

dimer	PL(S_0)	PL(S_1)	PL(exp)
D0	1.00	1.00	1.00
D1	0.22	0.32	2.92
D2	0.31	0.33	22.50

Table A3.4 S_1/S_0 energy gaps (in kcal/mol) at the inversion TS of the **D1** (*syn* and *anti*) and **D2** (*anti*) dimers estimated as: $\Delta E(S_1/S_0) = \Delta E(S_0{\rightarrow}S_1) - \lambda(S_1) + \Delta E(TS,S_1) - \Delta E(TS,S_0)$, where $\Delta E(S_0{\rightarrow}S_1)$ is the vertical gap at the FC geometry, $\lambda(S_1)$ is the reorganization energy of S_1, and $\Delta E(TS,S_0)$ and $\Delta E(TS,S_1)$ are the energy barriers at the S_0 transition state geometry on the S_0 and S_1 PESs, respectively.

dimer	conformer	$\Delta E(S_1/S_0)$
D1	*syn*	32.4
	anti	49.5
D2	*anti*	29.1

Table A3.5 Vertical transition energies to the lowest excited bright singlet state for the *anti*-**D2** dimer computed with different functionals and conditions. All values correspond to the 6-31G(d) basis set for the ωB97X-D/6-31G(d) optimized geometry in vacuum.

	TDDFT ωB97XD vacuum	TDA ωB97XD vacuum	TDDFT CAM-B3LYP vacuum	TDDFT ωB97XD DCM	experimental
bright S_n	S_1	S_3	S_1	S_1	-
eV	4.56	4.78	4.55	4.50	4.16
Δexp / eV	0.40	0.62	0.39	0.34	-
nm	272	259	273	276	298
f	0.20	0.20	0.19	0.26	-

Table A3.6 Vertical transition energies to the lowest excited bright singlet state for the *anti*-**D2** dimer computed at the TDDFT ωB97X-D level with different basis sets.

	6-31G(d)	6-31+G(d)	experimental
bright S_n	S_1	S_1	-
eV	4.50	4.42	4.16
Δexp / eV	0.34	0.26	-
nm	276	281	298
f	0.26	0.27	-

syn   anti   anti'

syn   anti   perp
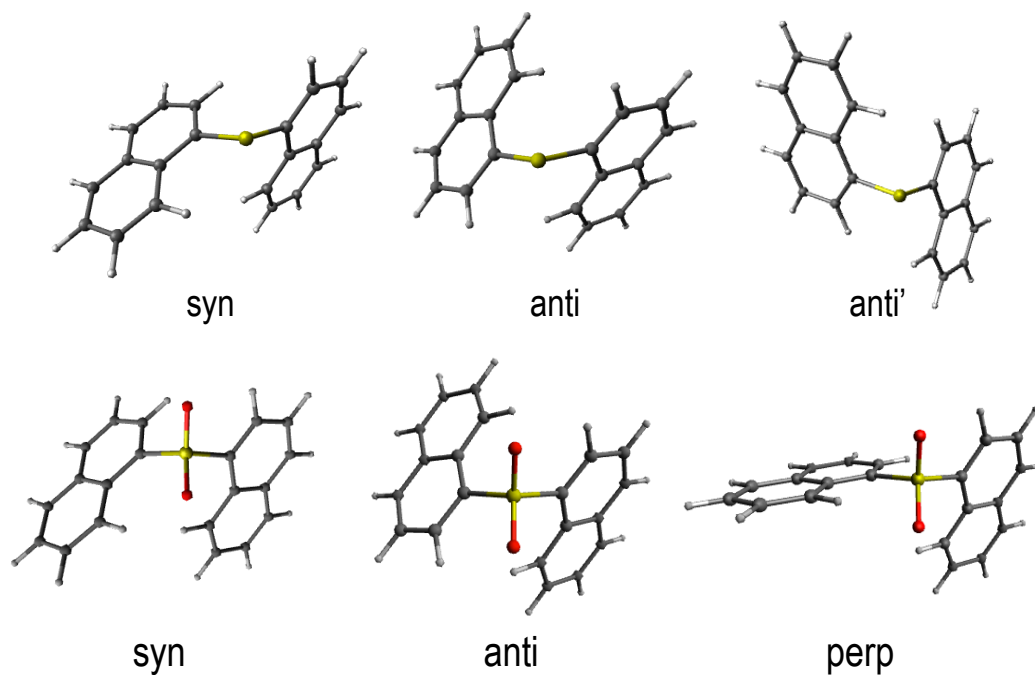
Figure A3.1 Low energy conformers for the ground state of **D0** (top) and **D2** (bottom) dimers.
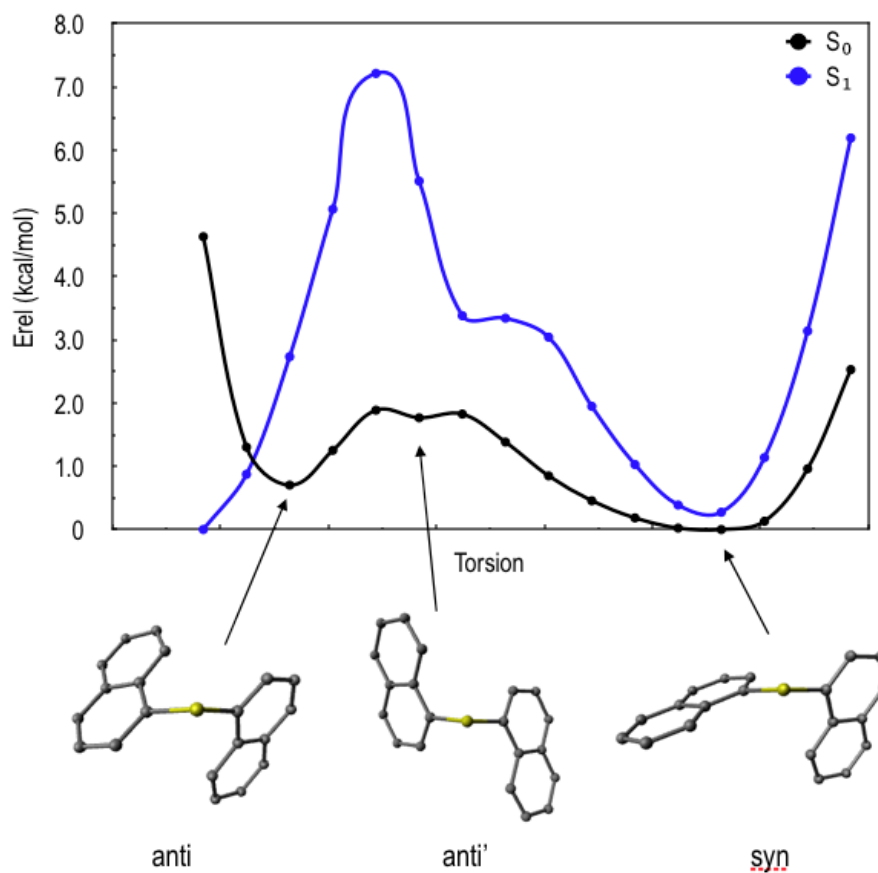
anti   anti'   syn

anti   anti'   syn

Figure A3.2   ersion between
conformers of   S.
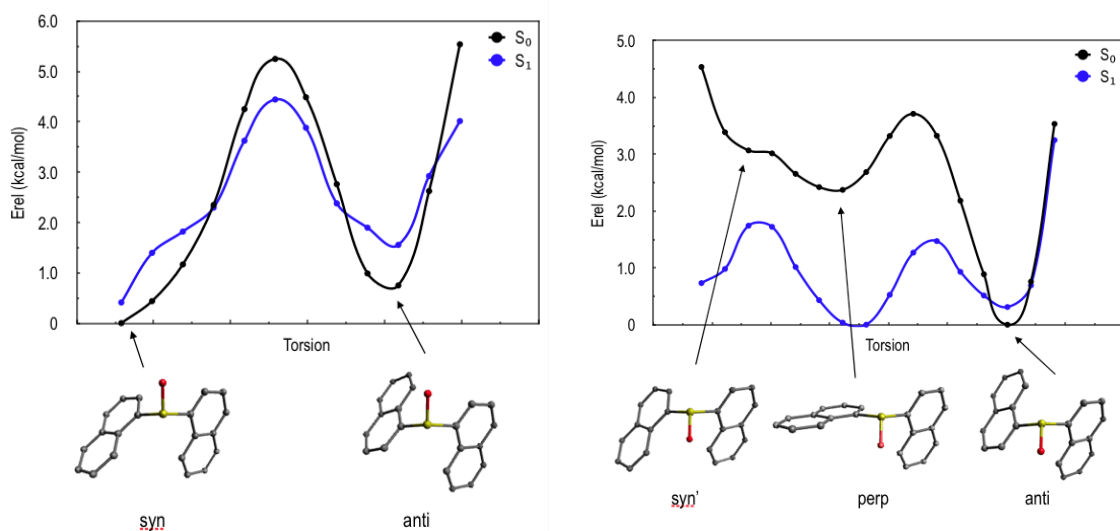
Figure A3.3 Ground and first excited state energy profiles for the interconversion between conformers of the **D1** dimer. All structures have been relaxed on the ground state PES.
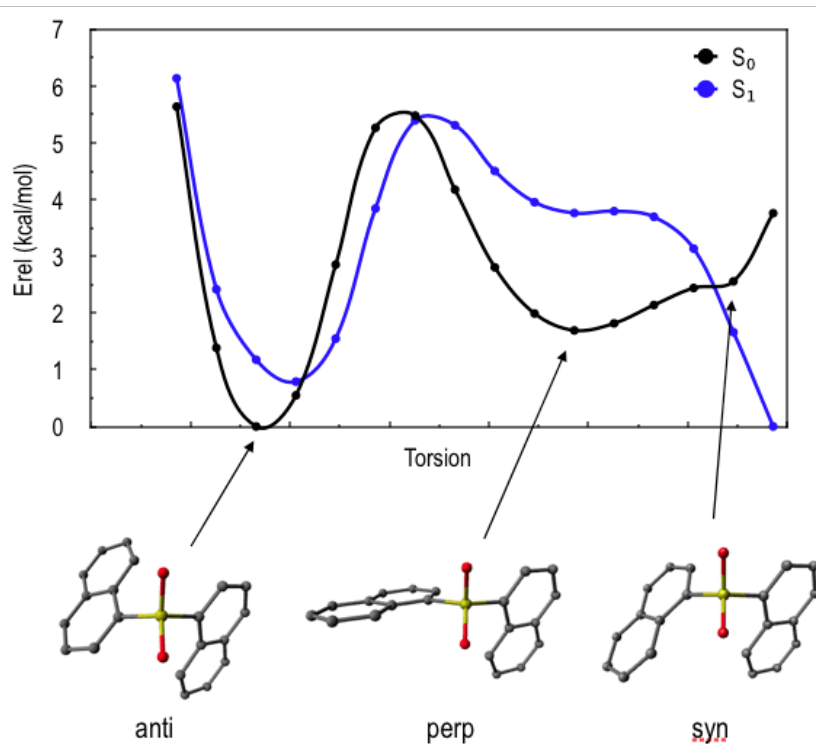
Figure A3.4 Ground and first excited state energy profiles for the interconversion between conformers of the **D2** dimer. All structures have been relaxed on the ground state PES.
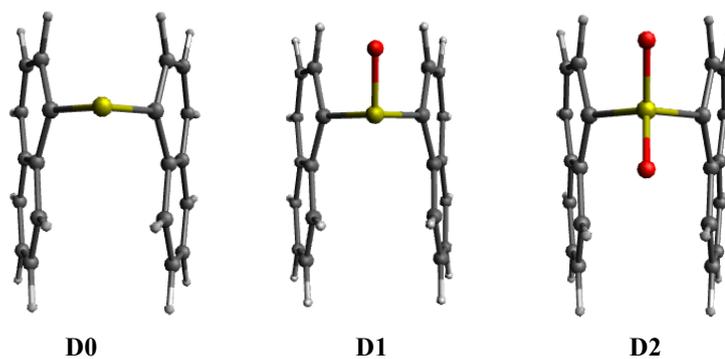
Figure A3.5 M... ...the ...ic sta...
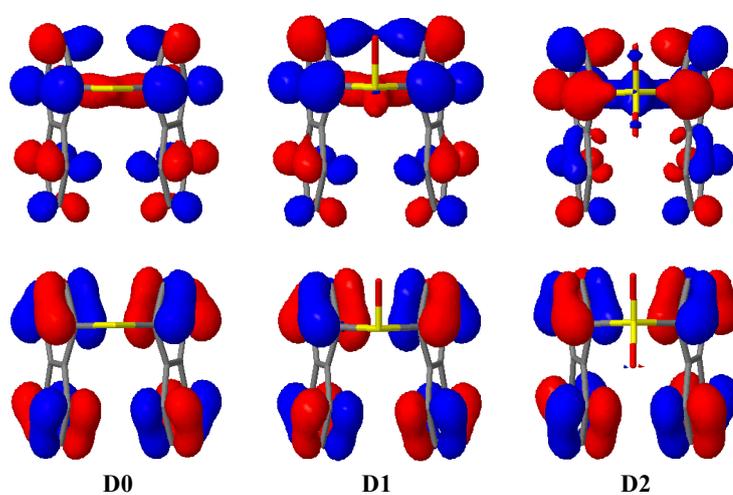
Figure A3.6 ...rbit... ma... ...n contribution of **Dn** excime...s.
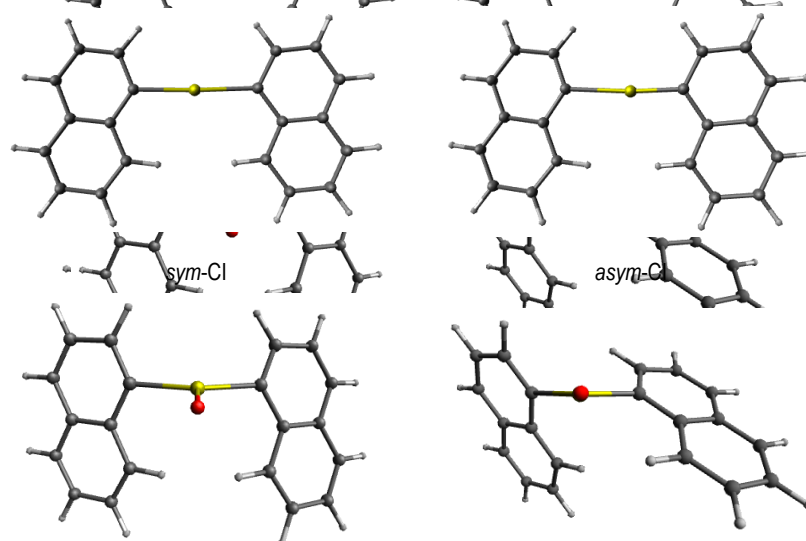
Figure A3.7 Molecular structures of **D0** (top) and **D1** (bottom) dimers at the *sym*-CI and *asym*-CI.

7. References

(1) Hedley, G. J.; Ruseckas, A.; Samuel, I. D. W. *Chem. Rev.* **2017**, *117*, 796.

(2) Heliatek www.heliatek.com (april 2017).

(3) NREL Best Research-Cell Efficiencies, www.nrel.gov/ncpv/images/efficiency_chart.jpg (april 2017).

(4) Rettig, W. *Angew. Chem., Int. Ed. Engl.* **1986**, *25*, 971.

(5) Grabowski, Z. R.; Rotkiewicz, K.; Rettig, W. *Chem. Rev.* **2003**, *103*, 3899.

(6) Bartynski, A. N.; Gruber, M.; Das, S.; Rangan, S.; Mollinger, S.; Trinh, C.; Bradforth, S. E.; Vandewal, K.; Salleo, A.; Bartynski, R. A.; Bruetting, W.; Thompson, M. E. *J. Am. Chem. Soc.* **2015**, *137*, 5397.

(7) Fyfe, D. *Nat. Photon.* **2009**, *3*, 453.

(8) Santato, C.; Cicoira, F.; Martel, R. *Nat. Photon.* **2011**, *5*, 392.

(9) Kulkarni, A. P.; Tonzola, C. J.; Babel, A.; Jenekhe, S. A. *Chem. Mater.* **2004**, *16*, 4556.

(10) Christensen, P. R.; Nagle, J. K.; Bhatti, A.; Wolf, M. O. *J. Am. Chem. Soc.* **2013**, *135*, 8109.

(11) Cruz, C. D.; Christensen, P. R.; Chronister, E. L.; Casanova, D.; Wolf, M. O.; Bardeen, C. J. *J. Am. Chem. Soc.* **2015**, *137*, 12552.

(12) Becker, R. S.; Seixas de Melo, J.; Maçanita, A. L.; Elisei, F. *J. Phys. Chem.* **1996**, *100*, 18683.

(13) Rossi, R.; Ciofalo, M.; Carpita, A.; Ponterini, G. *J. Photochem. Photobiol., A* **1993**, *70*, 59.

(14) Chai, J.-D.; Head-Gordon, M. *Phys. Chem. Chem. Phys.* **2008**, *10*, 6615.

(15) Hariharan, P. C.; Pople, J. A. *Theor. Chim. Acta* **1973**, *28*, 213.

(16) Franci, M. M.; Pietro, W. J.; Hehre, W. J. *J. Chem. Phys.* **1982**, *77*, 3654.

(17) Clark, T.; Chandrasekhar, J.; Spitznagel, G. W.; Schleyer, P. V. R. *J. Comput. Chem.* **1983**, *4*, 294.

(18) Chipman, D. M. *J. Chem. Phys.* **2000**, *112*, 5558.

(19) Cancès, E.; Mennucci, B. *J. Chem. Phys.* **2001**, *114*, 4744.

(20) Mead, C. A.; Truhlar, D. G. *J. Chem. Phys.* **1982**, *77*, 6090.

(21) Subotnik, J. E.; Cave, R. J.; Steele, R. P.; Shenvi, N. *J. Chem. Phys.* **2009**, *130*, 234102.

(22) Edmiston, C.; Ruedenberg, K. *Rev. Mod. Phys.* **1963**, *35*, 457.

(23) Levine, B. G.; Ko, C.; Quenneville, J.; Martĺnez, T. J. *Mol. Phys.* **2006**, *104*, 1039.

(24) Shao, Y.; Head-Gordon, M.; Krylov, A. I. *J. Chem. Phys.* **2003**, *118*, 4807.

(25) Bernard, Y. A.; Shao, Y.; Krylov, A. I. *J. Chem. Phys.* **2012**, *136*, 204103.

(26) *Advanced Series in Physical Chemistry, Conical Intersections: Electronic Structure, Dynamics and Spectroscopy*; World Scientific, 2004; Vol. 15.

(27) Minezawa, N.; Gordon, M. S. *J. Phys. Chem. A* **2009**, *113*, 12749.

(28) Nikiforov, A.; Gamez, J. A.; Thiel, W.; Huix-Rotllant, M.; Filatov, M. *J. Chem. Phys.* **2014**, *141*, 124122.

(29) Herbert, J. M.; Zhang, X.; Morrison, A. F.; Liu, J. *Acc. Chem. Res.* **2016**, *49*, 931.

(30) Becke, A. D. *Phys. Rev. A* **1988**, *38*, 3098.

(31) Lee, C.; Yang, W.; Parr, R. G. *Phys. Rev. B* **1988**, *37*, 785.

(32) Maeda, S.; Ohno, K.; Morokuma, K. *J. Chem. Theory Comput.* **2010**, *6*, 1538.

(33) Zhang, X.; Herbert, J. M. *J. Phys. Chem. B* **2014**, *118*, 7806.

(34) Shao, Y.; Gan, Z.; Epifanovsky, E.; Gilbert, A. T. B.; Wormit, M.; Kussmann, J.; Lange, A. W.; Behn, A.; Deng, J.; Feng, X.; Ghosh, D.; Goldey, M.; Horn, P. R.; Jacobson, L. D.; Kaliman, I.; Khaliullin, R. Z.; Kuś, T.; Landau, A.; Liu, J.; Proynov, E. I.; Rhee, Y. M.; Richard, R. M.; Rohrdanz, M. A.; Steele, R. P.; Sundstrom, E. J.; Woodcock, H. L.; Zimmerman, P. M.; Zuev, D.; Albrecht, B.; Alguire, E.; Austin, B.; Beran, G. J. O.; Bernard, Y. A.; Berquist, E.; Brandhorst, K.; Bravaya, K. B.; Brown, S. T.; Casanova, D.; Chang, C.-M.; Chen, Y.; Chien, S. H.; Closser, K. D.; Crittenden, D. L.; Diedenhofen, M.; DiStasio, R. A.; Do, H.; Dutoi, A. D.; Edgar, R. G.; Fatehi, S.; Fusti-Molnar, L.; Ghysels, A.; Golubeva-Zadorozhnaya, A.; Gomes, J.; Hanson-Heine, M. W. D.; Harbach, P. H. P.; Hauser, A. W.; Hohenstein, E. G.; Holden, Z. C.; Jagau, T.-C.; Ji, H.; Kaduk, B.; Khistyaev, K.; Kim, J.; Kim, J.; King, R. A.; Klunzinger, P.; Kosenkov, D.; Kowalczyk, T.; Krauter, C. M.; Lao, K. U.; Laurent, A. D.; Lawler, K. V.; Levchenko, S. V.; Lin, C. Y.; Liu, F.; Livshits, E.; Lochan, R. C.; Luenser, A.; Manohar, P.; Manzer, S. F.; Mao, S.-P.; Mardirossian, N.; Marenich, A. V.; Maurer, S. A.; Mayhall, N. J.; Neuscamman, E.; Oana, C. M.; Olivares-Amaya, R.; O'Neill, D. P.; Parkhill, J. A.; Perrine, T. M.; Peverati, R.; Prociuk, A.; Rehn, D. R.; Rosta, E.; Russ, N. J.; Sharada, S. M.; Sharma, S.; Small, D. W.; Sodt, A. *Mol. Phys.* **2015**, *113*, 184.

(35) Bearpark, M. J.; Robb, M. A.; Bernhard Schlegel, H. *Chem. Phys. Lett.* **1994**, *223*, 269.

(36)Cubbage, J. W.; Jenks, W. S. *J. Phys. Chem. A* **2001**, *105*, 10588.

(37)Kathayat, R. S.; Yang, L.; Sattasathuchana, T.; Zoppi, L.; Baldridge, K. K.; Linden, A.; Finney, N. S. *J. Am. Chem. Soc.* **2016**, *138*, 15889.

(38)Mislow, K.; Axelrod, M.; Rayner, D. R.; Gotthardt, H.; Coyne, L. M.; Hammond, G. S. *J. Am. Chem. Soc.* **1965**, *87*, 4958.

(39)Guo, Y.; Jenks, W. S. *J. Org. Chem.* **1997**, *62*, 857.

(40)Lindquist, B. A.; Woon, D. E.; Dunning, T. H. *J. Phys. Chem. A* **2014**, *118*, 1267.

(41)Vos, B. W.; Jenks, W. S. *J. Am. Chem. Soc.* **2002**, *124*, 2544.

(42)Suits, A. G. *Acc. Chem. Res.* **2008**, *41*, 873.

(43)Parr, R. G. In *Horizons of Quantum Chemistry: Proceedings of the Third International Congress of Quantum Chemistry Held at Kyoto, Japan, October 29 - November 3, 1979*; Fukui, K., Pullman, B., Eds.; Springer Netherlands: Dordrecht, 1980, p 5.

(44)Ziegler, T. *Chem. Rev.* **1991**, *91*, 651.

(45)Casida, M. E. *Time-dependent density-functional response theory for molecules*; World Scientific: Singapure, 1995; Vol. 1.

(46)Runge, E.; Gross, E. K. U. *Phys. Rev. Lett.* **1984**, *52*, 997.

(47)Frisch, M. J.; Trucks, G. W.; Schlegel, H. B.; Scuseria, G. E.; Robb, M. A.; Cheeseman, J. R.; Scalmani, G.; Barone, V.; Mennucci, B.; Petersson, G. A.; Nakatsuji, H.; Caricato, M.; Li, X.; Hratchian, H. P.; Izmaylov, A. F.; Bloino, J.; Zheng, G.; Sonnenberg, J. L.; Hada, M.; Ehara, M.; Toyota, K.; Fukuda, R.; Hasegawa, J.; Ishida, M.; Nakajima, T.; Honda, Y.; Kitao, O.; Nakai, H.; Vreven, T.; Montgomery Jr., J. A.; Peralta, J. E.; Ogliaro, F.; Bearpark, M. J.; Heyd, J.; Brothers, E. N.; Kudin, K. N.; Staroverov, V. N.; Kobayashi, R.; Normand, J.; Raghavachari, K.; Rendell, A. P.; Burant, J. C.; Iyengar, S. S.; Tomasi, J.; Cossi, M.; Rega, N.; Millam, N. J.; Klene, M.; Knox, J. E.; Cross, J. B.; Bakken, V.; Adamo, C.; Jaramillo, J.; Gomperts, R.; Stratmann, R. E.; Yazyev, O.; Austin, A. J.; Cammi, R.; Pomelli, C.; Ochterski, J. W.; Martin, R. L.; Morokuma, K.; Zakrzewski, V. G.; Voth, G. A.; Salvador, P.; Dannenberg, J. J.; Dapprich, S.; Daniels, A. D.; Farkas, Ö.; Foresman, J. B.; Ortiz, J. V.; Cioslowski, J.; Fox, D. J.; Gaussian, Inc.: Wallingford, CT, USA, 2009.